Winter 2-12-2018

Atmospheric chemistry of CH_3CHO: the hydrolysis of CH_3CHO catalyzed by H_2SO_4

Ellen Mitchell
Bridgewater College, emitchel@bridgewater.edu

Xing-Feng Tan
Guizhou University

Bo Long
Guizhou University

Wei-Jun Zhang
Chinese Academy of Sciences

Zheng-Wen Long
Guizhou University

Recommended Citation
Phys. Chem. Chem. Phys., 2018,20, 7701-7709

PCCP

PAPER

View Article Online
View Journal

Cite this: DOI: 10.1039/c7cp07312g

Atmospheric chemistry of CH_3CHO: the hydrolysis of CH_3CHO catalyzed by H_2SO_4†

Xing-Feng Tan,[a] Bo Long,*[b] Da-Sen Ren,[b] Wei-Jun Zhang,[cd] Zheng-Wen Long[e] and Ellen Mitchell*[f]

Elucidating atmospheric oxidation mechanisms and the reaction kinetics of atmospheric compounds is of great importance and necessary for atmospheric modeling and the understanding of the formation of atmospheric organic aerosols. While the hydrolysis of aldehydes has been detected in the presence of sulfuric acid, the reaction mechanism and kinetics remain unclear. Herein, we use electronic structure methods with CCSD(T)/CBS accuracy and canonical variational transition state theory combined with small-curvature tunneling to study the reaction mechanism and kinetics of the hydrolysis of CH_3CHO. The calculated results show that the hydrolysis of CH_3CHO needs to overcome an energy barrier of 37.21 kcal mol^{-1}, while the energy barrier is decreased to −9.79 kcal mol^{-1} with a sulfuric acid catalyst. In addition, the calculated kinetic results show that the $H_2SO_4\cdots H_2O$ + CH_3CHO reaction is faster than H_2SO_4 + $CH_3CHO\cdots H_2O$. Additionally, the $H_2SO_4\cdots H_2O$ + CH_3CHO reaction can play an important role in the sink of CH_3CHO below 260 K occurring during the night period when OH, H_2SO_4, and H_2O concentrations are 10^4, 10^8, and 10^{17} molecules cm^{-3}, respectively, because it can compete well with the CH_3CHO + OH reaction. There are wide implications in atmospheric chemistry from these findings because of the potential importance of the catalytic effect of H_2SO_4 on the hydrolysis of CH_3CHO in the atmosphere and in the formation of secondary organic aerosols.

Received 29th October 2017,
Accepted 12th February 2018

DOI: 10.1039/c7cp07312g

rsc.li/pccp

1. Introduction

Acetaldehyde (CH_3CHO) is an important member of carbonyl compounds in the atmosphere. Its concentration is slightly lower than formaldehyde. Acetaldehyde is released into the atmosphere from both anthropogenic and natural sources.[1,2] For example, the largest source of acetaldehyde is hydrocarbon oxidation with the emission of 128 Tg a^{-1}.[2] The concentration of acetaldehyde is about 0.70 ppb[3,4] in the United States and Europe, whereas its concentration is very high in China and Brazil at about 15.9 ppb[5] and 45.60 ppb,[6,7] respectively. Acetaldehyde plays critical roles in the atmosphere because it is an important source of ozone (O_3), peroxyacetyl nitrate,[8] and HO_x radicals.[9] Given the abundance of acetaldehyde in the atmosphere, it is of great necessity to fully investigate its sources, sinks, and reactivities to elucidate its roles in the atmospheric environment.

Acetaldehyde mainly reacts with OH and undergoes UV photolysis in the atmosphere.[10] In addition, the photochemistry of acetaldehyde is of particular importance because it provides a new potential pathway for the production of atmospheric acid.[11] Interest has risen in the gas-phase hydrolysis of some species in the atmosphere because of very recent experimental investigations showing that the hydrolysis of methylglyoxal occurs in the gas-phase.[12] Moreover, theoretical methods have been used to study the reaction mechanism and kinetics for the gas-phase hydrolysis of atmospheric molecules catalyzed by atmospheric acids.[13–24] For example, the gas-phase hydrolysis of SO_3 is catalyzed *via* HCOOH, H_2SO_4, and HNO_3.[13,14,22,25] However, in theory, single point energies in the hydrolysis of atmospheric molecules have mainly been calculated using CCSD(T)/aug-cc-pVTZ,[24]

[a] School of Mechatronics Engineering, Guizhou Minzu University, Guiyang, 550025, China
[b] School of Materials Science and Engineering, Guizhou Minzu University, Guiyang, 550025, China. E-mail: longbo@gzmu.edu.cn, wwwltcommon@sina.com
[c] Laboratory of Atmospheric Physico-Chemistry, Anhui Institute of Optics and Fine Mechanics, Chinese Academy of Sciences, Hefei, 230031, China
[d] Key Laboratory of Atmospheric Composition and Optical Radiation, Anhui Institute of Optics and Fine Mechanics, Chinese Academy of Sciences, Hefei, 230031, China
[e] Department of Physics, Guizhou University, Guiyang, 550025, China
[f] Department of Chemistry, Bridgewater College, Bridgewater, VA, 22812, USA. E-mail: emitchel@bridgewater.edu

† Electronic supplementary information (ESI) available: The scale factors are listed in Table S1, the binding energies are provided in Table S2, Cartesian coordinates of optimized structures are present in Table S3, the calculated frequencies of optimized structures are given in Table S4, the total energies of optimized structures are listed in Table S5, the optimized geometries of sulfuric acid, the $CH_3CHO\cdots H_2O$ complexes and the $H_2SO_4\cdots H_2O$ complexes are given in Fig. S1, the temperature-dependent equilibrium constant (K_{eqC1A}) between 190 and 350 K is given in Fig. S2, and intrinsic reaction coordinate results are provided in Fig. S3 and S4. See DOI: 10.1039/c7cp07312g

which may lead to some uncertainties of reaction energy barriers and thus further affect rate constant calculations. Additionally, transition state theory has been used to calculate rate constants, which is less accurate than canonical variational transition state theory. Therefore, exploring the gas-phase hydrolysis of acetaldehyde is of particular interest and necessary for a more complete estimation of the sinks of acetaldehyde in the atmosphere.

The hydrolysis of acetaldehyde catalyzed by sulfuric acid is theoretically investigated using post-CCSD(T) electronic structure benchmarks, a validated density functional method for direct kinetics calculations, canonical variational transition state theory (CVT) with small-curvature tunneling (SCT), coupled-torsion anharmonicity, and high-frequency anharmonicity. Sulfuric acid is chosen as a catalyst to catalyze the hydrolysis of acetaldehyde because previous investigations have indicated that sulfuric acid can play a strong catalytic role in the hydrolysis of SO_3, HCHO, and SO_2.[16,19,22] Moreover, sulfuric acid also plays an important role in catalyzing the reactions of epoxides responsible for atmospheric nanoparticle growth.[26] Additionally, acetaldehyde becomes easily hydrated and forms acetal oligomers responsible for the formation of secondary organic aerosols in the aqueous phase.[27] This study suggests that sulfuric acid plays a remarkable catalytic role in the gas-phase hydrolysis of acetaldehyde. The present results not only provide new insights into the formation of secondary organic aerosols in the hydrolysis of acetaldehyde, but also show that the gas-phase hydrolysis of acetaldehyde plays a critical role in the sink of acetaldehyde under some atmospheric conditions.

2. Computational methods

Benchmark calculations were carried out to determine whether the theoretical methods used herein are reliable. We have shown that the W3X-L//QCISD/VTZ theoretical method can produce rate constants with experimental accuracy in the Criegee intermediates + H_2O reactions.[28] The H_2O + CH_3CHO reaction was optimized at the QCISD/VTZ level of theory. The corresponding frequencies of the H_2O + CH_3CHO reaction were computed at the same level to show that the reactant, complex, and product have no imaginary frequencies and the transition state has only one imaginary frequency. The single point energies of the H_2O + CH_3CHO reaction were refined using W3X-L,[29] W2X,[29] CCSD(T)-F12a/VTZ-F12,[30–33] and CCSD(T)/AVTZ[34,35] theoretical methods at the QCISD/VTZ[36]-optimized geometries to examine the effects of basis sets.

Geometry optimizations and harmonic vibrational frequency calculations of all the reactants, pre- and postreactive complexes, transition states, and products were performed using the M06-2X[37] functional with the MG3S basis set.[38] The M06-2X functional has been shown to be adequately reliable for predicting the geometries and frequencies of the stationary points in the literature.[15,19,39] The transition state has only a single imaginary frequency, while other stationary points have positive frequencies. Intrinsic reaction coordinate (IRC) computations[40,41] were carried out to determine whether the designated transition state connects appropriate prereactive and postreactive complexes along the reaction coordinate. To improve the relative energies, single point energy calculations were executed using the CCSD(T)-F12a/VTZ-F12 theoretical method at the M06-2X/MG3S-optimized geometries.

To perform direct kinetics calculations, the MPWB1K functional[42] was employed to reinvestigate sulfuric acid-catalyzed hydrolysis of CH_3CHO at the MG3S basis set. The direct kinetics calculations by MPWB1K/MG3S were performed using canonical variational transition state theory with small-curvature tunneling (CVT/SCT).[43–51] Rate constants were computed utilizing the following formula (1)

$$k = \frac{k_{TST}^{HL}}{k_{TST}^{LL}} k_{CVT/SCT}^{LL} = k_{TST}^{HL} \frac{\kappa_{SCT}^{LL} k_{CVT}^{LL}}{k_{TST}^{LL}} = k_{TST}^{HL} \kappa_{SCT}^{LL} \Gamma_{CVT}^{LL} \quad (1)$$

where $k_{CVT/SCT}^{LL}$ represents the rate constant calculated using canonical variational transition state theory with small-curvature tunneling at the MPWB1K/MG3S level, k_{TST}^{HL} and k_{TST}^{LL} stand for the rate constants calculated by transition state theory at the CCSD(T)-F12a/VTZ-F12//M06-2X/MG3S and MPWB1K/MG3S levels, respectively, κ_{SCT}^{LL} is the tunneling coefficient at the MPWB1K/MG3S level, Γ_{CVT}^{LL} is the ratio of k_{CVT}^{LL} to k_{TST}^{LL}, and LL and HL stand for respectively lower and higher levels of the electronic structure method. Herein LL and HL are MPWB1K/MG3S and CCSD(T)-F12a/VTZ-F12//M06-2X/MG3S, respectively. A similar method was used to correct the rate constants by canceling the uncertainties of barrier heights in our previous investigation of the Criegee intermediates + H_2O reactions[28] and the HO_2 + FCHO reaction,[52] where we used W3X-L single point energies. However, it is noted that the barrier heights calculated using CCSD(T)-F12a/VTZ-F12//M06-2X/MG3S herein still may have an error bar of 0.5 kcal mol^{-1}.

Scale factors,[53] which are provided in Table S1 (ESI†), were used in the thermochemistry and kinetics calculations to correct anharmonicity and systematic errors in high frequencies. In addition, we calculated the torsional anharmonicity and torsion-rotation coupling[54,55] in the MSTor code.[56] The electronic structure calculations were executed using Gaussian 09,[57] Molpro 2012,[58] and MRCC,[59,60] while the rate constants were executed using Polyrate 2016-2A[61] and Gaussrate2016.[62]

3. Results and discussion

3.1 The reaction of acetaldehyde with water

The CH_3CHO + H_2O reaction[18] is reinvestigated to estimate the reliability of the theoretical methods used here and the catalytic role of sulfuric acid in the gas-phase hydrolysis of CH_3CHO. The CH_3CHO + H_2O reaction occurs *via* the prereactive C1A complex and proceeds through the transition state TS1 responsible for the formation of products P as characterized in Fig. 1 and 2. There are two complexes between CH_3CHO and H_2O as shown in Fig. S1 (ESI†). Table S2 (ESI†) indicates that C1A is more stable than C1B by about 0.5 kcal mol^{-1} calculated using CCSD(T)-F12a/VTZ-F12//M06-2X/MG3S. We consider two structures,

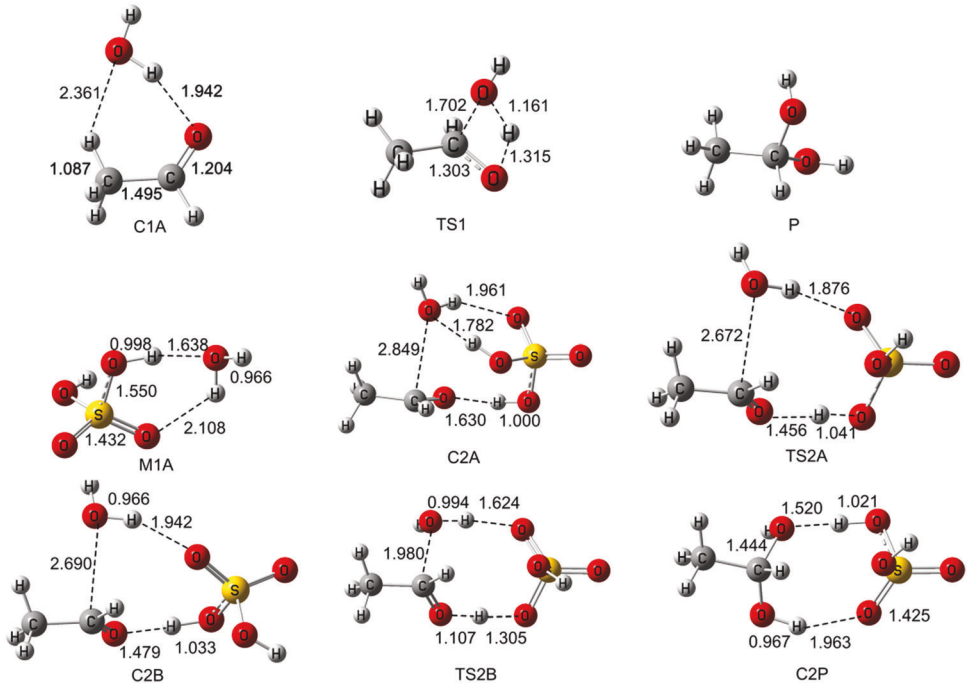

Fig. 1 Selected geometrical parameters of the optimized reactants, transition states, products, and complexes at the M06-2X/MG3S level of theory.

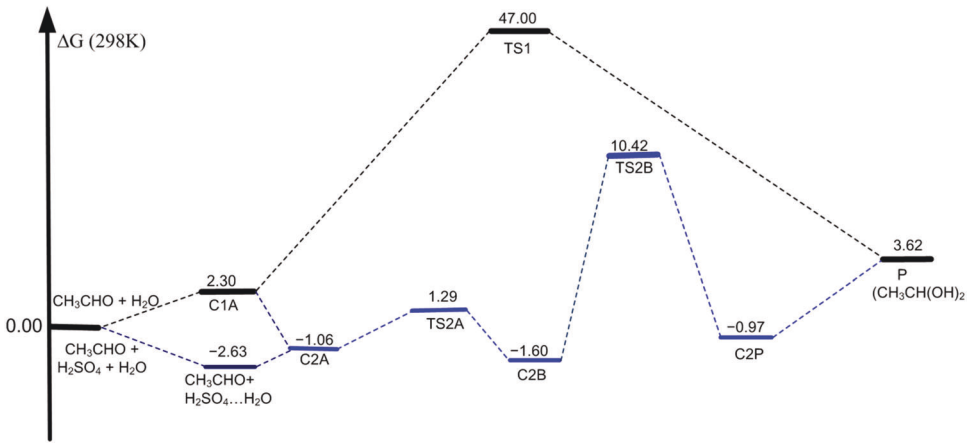

Fig. 2 The free energy potential profile for the $CH_3CHO + H_2O$ and $CH_3CHO + H_2SO_4 + H_2O$ reactions at the CCSD(T)-F12a/VTZ-F12//M06-2X/MG3S level.

C1A and C1B, to compute the conformational–rovibrational partition function in the equilibrium constant calculations.

In Table 1, the mean unsigned error (MUE) of W2X//QCISD/VTZ is 0.02 kcal mol^{-1}, compared with our best W3X-L//QCISD/VTZ theoretical method, revealing that the post-CCSD(T) calculation is negligible because the W3X-L theoretical method is equal to W2X plus the post-CCSD(T) theoretical method.[29] Our previous investigations have used the differences in single point energy calculations between W2X and W3X-L to estimate the multireference features of reaction systems.[28,63] Thus, this shows that the $CH_3CHO + H_2O$ reaction has no obvious multireference features.

Table 1 also indicates that the CCSD(T)-F12a/VTZ-F12 theoretical method approaches the CCSD(T)/CBS accuracy because

Table 1 The binding energies (ΔE^a, 0 K), energy barriers (ΔE^b, 0 K), and reaction energies (ΔE^c, 0 K) of the $CH_3CHO + H_2O$ reaction at different theoretical methods with zero-point correction involved and mean unsigned error (MUE) (in kcal mol^{-1})

Methods	ΔE^a	ΔE^b	ΔE^c	MUE[d]
W3X-l//QCISD/VTZ	−3.97	37.49	−5.80	0.00
W2X//QCISD/VTZ	−3.95	37.50	−5.97	0.02
CCSD(T)-F12a/VTZ-F12//QCISD/VTZ	−3.94	37.42	−5.91	0.07
CCSD(T)/AVTZ//QCISD/VTZ	−4.12	36.84	−6.0	0.33
CCSD(T)-F12a/VTZ-F12//M06-2X/MG3S	−4.55	37.21	−6.14	0.47

[a] The binding energies with respect to CH_3CHO and H_2O. [b] The energy barriers with respect to $CH_3CHO + H_2O$. [c] The reaction barriers with respect to $CH_3CHO + H_2O$. [d] Mean unsigned error averaged over the three previous columns.

the CCSD(T)-F12a/VTZ-F12//QCISD/VTZ results have excellent agreement with those calculated using W2X//QCISD/VTZ. Additionally, it is noted that although the MUE of CCSD(T)-F12a/VTZ-F12//M06-2X/MG3S is about 0.47 kcal mol^{-1}, it is chosen to study the hydrolysis of CH_3CHO catalyzed by sulfuric acid because the energy barrier calculated by CCSD(T)-F12a/VTZ-F12//M06-2X/MG3S is about 0.3 kcal mol^{-1} lower than that of W3X-L//QCISD/VTZ for the CH_3CHO + H_2O reaction. The barrier height of the CH_3CHO + H_2O reaction is calculated to be 37.21 kcal mol^{-1} at the CCSD(T)-F12a/VTZ-F12//M06-2X/MG3S level, which indicates that the direct reaction of CH_3CHO with H_2O is negligible under atmospheric conditions. The barrier height (37.21 kcal mol^{-1}) of TS1 at the CCSD(T)-F12a/VTZ-F12//M06-2X/MG3S level is about 1.5 kcal mol^{-1} lower than that of the CCSD(T)/6-311++G(2df,2p)//MP2/6-311++G(2df,2p) level.[18] Moreover, the CCSD(T)/aug-cc-pVTZ//QCISD/VTZ theoretical method underestimates the reaction barrier by about 0.58 kcal mol^{-1}, compared with the W2X//QCISD/VTZ value. Thus, the result also shows that the CCSD(T) theoretical method with the larger basis sets than aug-cc-pVTZ is needed to reliably describe the energy barrier of the CH_3CHO + H_2O reaction. The discussion below is based on the CCSD(T)-F12a/VTZ-F12//M06-2X/MG3S results unless otherwise stated.

3.2 The hydrolysis of acetaldehyde catalyzed by sulfuric acid

When sulfuric acid is introduced as a catalyst into the reaction of CH_3CHO with H_2O, there are two possible entrance channels, $CH_3CHO\cdots H_2O$ + H_2SO_4 and CH_3CHO + $H_2SO_4\cdots H_2O$, which are described in Fig. 1 and 2.

When the $CH_3CHO\cdots H_2O$ complex and H_2SO_4 act as reactants, the reaction occurs in one elementary step, which is similar to the HCOOH-catalyzed hydrolysis of CH_3CHO and HCHO,[15,18] as well as HNO_3 and HCOOH-catalyzed hydrolysis of SO_3.[13,14,25] The reaction starts with the formation of the prereactive complex C2B and proceeds through the corresponding transition state TS2B responsible for the formation of the postreactive complex C2P as described in Fig. 2. In Table 2, the binding energy of the $CH_3CHO\cdots H_2O$ complex is calculated to be −4.55 kcal mol^{-1}, which agrees well with the calculated value of −4.6 kcal mol^{-1} at the CCSD(T)/6-311++G(2df,2p)//MP2/6-311++G(2df,2p) level.[18] The prereactive C2B complex is an eight-membered ring structure where there are two hydrogen-bonded interactions and a van der Waals interaction. One of these hydrogen bonding interactions is very strong as indicated by an estimated hydrogen-bonded distance of 1.479 Å. This is again confirmed by the calculated binding energy of −18.51 kcal mol^{-1}, revealing a strong interaction in the ternary C2B complex (Table 2). Moreover, the binding energy (−18.51 kcal mol^{-1}) of C2B is about 1.8 kcal mol^{-1} lower than that of the ternary complex formed by H_2SO_4, H_2O, and HCHO at the CCSD(T)/aug-cc-pV(T+d)Z level.[19]

The prereactive C2B complex undergoes a unimolecular isomerization through TS2B, resulting in the formation of C2P. In TS2B, this is a concerted reaction mechanism where the hydrogen atom of the OH group in sulfuric acid is transferred to the oxygen atom of the carbonyl group in CH_3CHO, the hydrogen atom of H_2O is migrated to the oxygen atom of a S═O group on the sulfuric acid, and simultaneously the OH group from H_2O is added to the carbonyl carbon of CH_3CHO, which is similar to the hydrolysis of HCHO catalyzed by sulfuric acid.[19] The O–H bond in sulfuric acid that bridges with the terminal oxygen atom of the C═O group in CH_3CHO in TS2B is lengthened to 1.305 Å from 1.033 Å in C2B, and the distance between the oxygen atom of H_2O and the carbon atom of the C═O group in CH_3CHO is shortened to 1.980 Å from 2.690 Å in C2B. It is particularly noted that the reaction barrier *via* TS2B is computed to be 8.72 kcal mol^{-1} with respect to the prereactive C2B complex (Table 2), which is about 3–6 kcal mol^{-1} lower than those of the other atmospheric acid-catalyzed hydrolyses of CH_3CHO.[18] The result shows that sulfuric acid plays a stronger catalytic role in the hydrolysis of CH_3CHO than other acid-catalysts. It is noted that the binding energy of the postreative C2P complex is 2.66 kcal mol^{-1} lower than that of C2B in Table 2.

Table 2 The binding, activated, and reaction energies (ΔE, 0 K), enthalpies (ΔH, 298 K), and free energies (ΔG, 298 K) for the hydrolysis of CH_3CHO catalyzed by H_2SO_4 with zero-point correction (ZPE) included (in kcal mol^{-1})

	M06-2X			CCSD(T)-F12a//M06-2X		
	ΔE^a	ΔH^a	ΔG^a	ΔE^b	ΔH^b	ΔG^b
$CH_3CHO + H_2O \rightarrow CH_3CH(OH)_2$						
$CH_3CHO + H_2O$	0.00	0.00	0.00	0.00	0.00	0.00
C1A($CH_3CHO\cdots H_2O$)	−5.01	−5.19	1.84	−4.55	−4.73	2.30
TS1	35.37	33.60	45.16	37.21	35.44	47.00
P($CH_3CH(OH)_2$)	−9.22	−10.88	−0.54	−6.14	−7.80	3.62
$CH_3CHO + H_2O + H_2SO_4 \rightarrow CH_3CH(OH)_2 + H_2SO_4$						
$CH_3CHO + H_2O + H_2SO_4$	0.00	0.00	0.00	0.00	0.00	0.00
C1A($CH_3CHO\cdots H_2O$) + H_2SO_4	−5.01	−5.19	1.84	−4.55	−4.73	2.30
CH_3CHO + M1A($H_2SO_4\cdots H_2O$)	−11.90	−12.52	−3.88	−10.65	−11.28	−2.63
C2A	−22.40	−23.05	−3.46	−20.00	−20.64	−1.06
TS2A	−19.85	−20.50	−1.33	−17.23	−17.88	1.29
C2B	−20.93	−21.12	−4.01	−18.51	−18.71	−1.60
TS2B	−13.81	−15.54	6.41	−9.79	−11.52	10.42
C2P	−25.69	−27.39	−5.49	−21.17	−22.87	−0.97
P($CH_3CH(OH)_2$) + H_2SO_4	−9.22	−10.88	−0.54	−6.14	−7.80	3.62

[a] ΔE, ΔH, and ΔG are obtained at the M06-2X/MG3S level. [b] ΔE, ΔH, and ΔG are calculated at the CCSD(T)-F12a/VTZ-F12//M06-2X/MG3S level.

When $H_2SO_4\cdots H_2O$ and CH_3CHO act as reactants, the $CH_3CHO + H_2SO_4\cdots H_2O$ reaction occurs in two steps as depicted in Fig. 2. Regarding H_2SO_4, there are two conformers with C_2 and C_s symmetry, respectively, as shown in Fig. S1 (ESI†). The most stable structure of sulfuric acid has C_2 symmetry, while the secondary stable structure has C_s symmetry. The calculated results show that the C_2 sulfuric acid is 1.04 kcal mol^{-1} lower than the C_s sulfuric acid (Table S2, ESI†), which is in good agreement with the previous values of about 1 kcal mol^{-1} reported in the literature.[64] In addition, there are four complexes between sulfuric acid and water as characterized in Fig. S1 (ESI†). The binding energies among the M1A, M1B, M1C, and M1D complexes are computed to be −10.65, −10.56, −9.50, and −8.94 kcal mol^{-1}, respectively, as listed in Table S2 (ESI†). This result indicates that the different isomers should be considered to illustrate the contribution of multistructural isomers to equilibrium constants.

The first step begins with the formation of the prereactive C2A complex, which transforms into the C2B product through the TS2A transition state, while the second step is C2B isomerization into C2P *via* TS2B, which has been discussed above. Herein, we focus on the first step because the second step has been previously discussed in the $CH_3CHO\cdots H_2O + H_2SO_4$ reaction. It is noted that C2A has a binding energy of −20.00 kcal mol^{-1}, which is about 1 kcal mol^{-1} lower than that of the corresponding complex in the $HCHO + H_2SO_4\cdots H_2O$ reaction.[19] Furthermore, the energy barrier of C2A isomerization into C2B is very low with a value of 2.77 kcal mol^{-1}, revealing that this process facilely occurs in the atmosphere. It is worth noting that the second step is the rate-determining step. Thus, it is reasonable that the first step was not considered in similar reactions.[18,21]

For direct kinetics calculations, the barrier heights associated with TS2B with respect to different pre-reactive complexes are estimated using the MPWB1K/MG3S method as listed in Table 3. The calculated results show that the MPWB1K/MG3S method is reliable for characterizing the $CH_3CHO + H_2O$ reaction catalyzed by sulfuric acid because the differences in energy between the CCSD(T)-F12a/VTZ-F12//M06-2X/MG3S and MPWB1K/MG3S methods are about 0.7 kcal mol^{-1} as shown in Table 3, while the error bar of M06-2X/MG3S is about 1.5 kcal mol^{-1}. Thus, the MPWB1K/MG3S theoretical method is utilized to do direct kinetics calculations of the $CH_3CHO + H_2O$ reaction catalyzed by sulfuric acid. In addition, we also use M06-2X/MG3S to do direct kinetics calculations to reveal how different functional methods influence the calculated rate constants.

Table 3 The energy barriers of the $CH_3CHO + H_2O$ reaction catalyzed by sulfuric acid relative to different prereactive complexes with zero-point correction involved (in kcal mol^{-1})

	Methods	
Barrier height	CCSD(T)-F12a/VTZ-F12//M06-2X/MG3S	MPWB1K/MG3S
$\Delta E^{\ddagger}$ (TS2B → C2A)	10.21	9.46
$\Delta E^{\ddagger}$ (TS2B → C2B)	8.72	8.49

3.3 Reaction kinetics

With regard to the reactions involving three molecules, we consider $H_2SO_4\cdots H_2O$ and CH_3CHO or $CH_3CHO\cdots H_2O$ and H_2SO_4. When $H_2SO_4\cdots H_2O$ and CH_3CHO are act as reactants, the ternary molecular reactions occur *via* the following reaction mechanism,

$$H_2O + H_2SO_4 \leftrightarrow H_2SO_4\cdots H_2O \quad (2)$$

$$H_2SO_4\cdots H_2O + CH_3CHO \rightarrow CH_3CH(OH)_2 + H_2SO_4 \quad (3)$$

while when $CH_3CHO\cdots H_2O$ and H_2SO_4 are considered to be reactants, the reaction mechanism is shown below.

$$H_2O + CH_3CHO \leftrightarrow CH_3CHO\cdots H_2O \quad (4)$$

$$CH_3CHO\cdots H_2O + H_2SO_4 \rightarrow CH_3CH(OH)_2 + H_2SO_4 \quad (5)$$

The rate *via* the reaction processes (2) and (3) is expressed in eqn (6)

$$\nu_1 = \frac{d[CH_3CH(OH)_2]}{dt} = K_{eq2}k_3[H_2SO_4][H_2O][CH_3CHO] \quad (6)$$

where K_{eq2} is the equilibrium constant for the formation of the $H_2SO_4\cdots H_2O$ complex from isolated H_2SO_4 and H_2O and k_3 represents the rate constant of eqn (3). The rate *via* eqn (4) and (5) is written in eqn (7)

$$\nu_2 = \frac{d[CH_3CH(OH)_2]}{dt} = K_{eq4}k_5[H_2SO_4][H_2O][CH_3CHO] \quad (7)$$

where K_{eq5} expresses the equilibrium constant for the formation of the $CH_3CHO\cdots H_2O$ complex from isolated CH_3CHO and H_2O and k_5 represents the rate constant of eqn (5). It is noted that the equilibrium constants K_{eq2} and K_{eq4} are computed using multistructural method with torsional anharmonicity, where different structures are considered to reflect the contribution to equilibrium constants. In addition, we do not consider how pressure effects affect the formation of these complexes investigated herein because there are no experimental results that show that the equilibrium constants of these complexes depend on pressure.

The computed rate constants are provided in Table 4. It is noted that k_3 and k_5 are computed using the formula (1) mentioned in Section 2. The bimolecular rate constants of the $H_2SO_4\cdots H_2O + CH_3CHO$ (k_3) and $H_2SO_4 + CH_3CHO\cdots H_2O$ (k_5) reaction were fitted using the following formulas[48]

$$k_3 = 1.154\times10^{-16}\left(\frac{T+25.583}{300}\right)^{1.002}\exp\left[-\frac{0.418(T+23.583)}{R(T^2+604.303)}\right] \quad (8)$$

$$k_5 = 8.736\times10^{-17}\left(\frac{T+51.051}{300}\right)^{-0.669}\exp\left[\frac{4.180(T+51.051)}{R(T^2+2606.209)}\right] \quad (9)$$

Table 4 The equilibrium constants (molecules cm^{-3}) and rate constants (cm^3 molecule^{-1} s^{-1}) at different temperatures

T/K	190	200	220	240	260	280	298	320
K_{eq2}[a]	1.6×10^{-13}	3.8×10^{-14}	3.1×10^{-15}	3.9×10^{-16}	6.8×10^{-17}	1.5×10^{-17}	4.7×10^{-18}	1.4×10^{-18}
K_{eq4}[a]	3.0×10^{-20}	1.7×10^{-20}	6.0×10^{-21}	2.6×10^{-21}	1.3×10^{-21}	7.4×10^{-22}	4.7×10^{-22}	2.9×10^{-22}
κ_{SCT}[b]	1.29	1.25	1.20	1.17	1.14	1.12	1.11	1.10
Γ_{CVT}[b]	0.62	0.64	0.68	0.71	0.74	0.76	0.77	0.79
κ_{SCT}[c]	1.31	1.27	1.22	1.18	1.15	1.13	1.12	1.10
Γ_{CVT}[c]	0.76	0.78	0.82	0.84	0.87	0.89	0.89	0.91
k_3[d]	2.4×10^{-17}	2.7×10^{-17}	3.3×10^{-17}	3.9×10^{-17}	4.6×10^{-17}	5.2×10^{-17}	5.8×10^{-17}	6.9×10^{-17}
k_5[d]	5.0×10^{-11}	2.4×10^{-11}	6.7×10^{-12}	2.3×10^{-12}	9.5×10^{-13}	4.4×10^{-13}	2.4×10^{-13}	1.3×10^{-13}
E_a[e]	0.84	0.85	0.89	0.92	0.96	0.99	1.03	1.07
E_a[f]	−5.53	−5.54	−5.55	−5.54	−5.54	−5.53	−5.52	−5.51
ν_1/ν_2	2.7	2.6	2.6	2.5	2.5	2.4	2.4	2.4
$K_{eq2}k_3/k_6$	1.3×10^{-19}	3.8×10^{-20}	4.5×10^{-21}	7.6×10^{-22}	1.7×10^{-22}	4.9×10^{-23}	1.8×10^{-23}	6.4×10^{-24}

[a] The values computed using CCSD(T)-F12a/VTZ-F12//M06-2X/MG3S. [b] The values computed using MPWB1K/MG3S. [c] The values computed using M06-2X/MG3S. [d] The values computed using the formula (1). [e] The activation energies of the $CH_3CHO + H_2SO_4\cdots H_2O$ reaction. [f] The activation energies of the $H_2SO_4 + CH_3CHO\cdots H_2O$ reaction.

It is noted that the rate constant values are given in cm^3 molecule^{-1} s^{-1}. The temperature-dependent activation energy was calculated from the fit as[65]

$$E_a = -R\frac{d\ln k}{d(1/T)} \quad (10)$$

The calculated results show that the rate constant of the $H_2SO_4 + CH_3CHO\cdots H_2O$ reaction is higher than that of the $H_2SO_4\cdots H_2O + CH_3CHO$ reaction, while the rate ratio ν_1/ν_2 of the $CH_3CHO + H_2O + H_2SO_4$ reaction shows that the entrance of $H_2SO_4\cdots H_2O + CH_3CHO$ is more important than that of $H_2SO_4 + CH_3CHO\cdots H_2O$ in the $CH_3CHO + H_2SO_4 + H_2O$ reaction because the rate ratio ν_1/ν_2 is 2.7–2.4 between 190 and 320 K (Table 4). In addition, the rate constant of the $H_2SO_4 + CH_3CHO\cdots H_2O$ reaction (k_5) has a negative temperature dependence, while the rate constant of the $CH_3CHO + H_2O\cdots H_2SO_4$ reaction (k_3) has a positive temperature dependence (Table 4 and Fig. 3). Moreover, the temperature-dependent rate constant of $H_2SO_4 + CH_3CHO\cdots H_2O$ is much higher than that of $H_2SO_4\cdots H_2O + CH_3CHO$ because the activation energy of $H_2SO_4 + CH_3CHO\cdots H_2O$ is −5.52 kcal mol^{-1} at 298 K, while the activation energy of $H_2SO_4\cdots H_2O + CH_3CHO$ is 1.03 kcal mol^{-1} at 298 K (Table 4). It is noted that K_{eq4} and k_5 have nonmonotonic temperature dependence of the equilibrium constant and the rate constant (Fig. 3). The multistructural torsional anharmonicity makes major contribution to the nonmonotonic temperature dependence of the equilibrium constant because the equilibrium constant of the single structural C1A complex has a monotonic temperature dependence as shown in Fig. S2 (ESI†). With regard to k_5, the nonmonotonic temperature dependence of the rate constant is caused by the negative barrier height (Table 2). For negative barrier reactions, the activation free energy is negative at low temperatures (at 0 K, activation free energy is equal to the zero-point correction included a barrier height, which is negative, and because the temperature is low, the entropic contribution can be neglected); at higher temperatures, the entropic effects start dominating, and the negative activation entropy leads to the increase of activation free energy, and when the activation energy is positive, one has positive temperature dependence on rate constants.

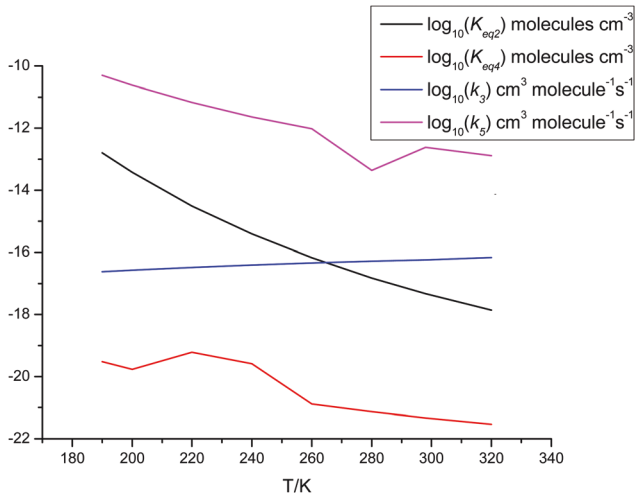

Fig. 3 The temperature-dependent equilibrium constants (K_{eq2} and K_{eq4}) and the rate constants (k_3 and k_5) between 190 and 320 K.

Tunneling slightly increases the rate constant, while the recrossing effects decrease the rate constant. For example, the rate constant is increased by 11% due to tunneling, while the rate constant is decreased to 77% because of recrossing effects at the MPWB1K/MG3S level and at 298 K (Table 4). It is noted that tunneling and recrossing effects slightly depend on temperature. Tunneling slightly increase with the decrease of temperature, while recrossing effects slightly increase with the decrease of temperature as listed in Table 4. Specifically, the calculated results using MPWB1K/MG3S indicate that the rate constant is increased by 29% and 10% due to tunneling, while the rate constant is decreased to 62% and 79% at 190, 320 K, respectively. Additionally, the calculated results also show that the tunneling is not sensitive to the barrier height because the M06-2X/MG3S and MPWB1K/MG3S tunneling coefficients (κ_{SCT}) are almost identical (Table 4). However, the recrossing effects are determined by the theoretical methods because there are some differences between the Γ_{CVT} values calculated using MPWB1K/MG3S and M06-2X/MG3S (Table 4). In particular, it is of great necessity to have a reliable functional to obtain rate constants.

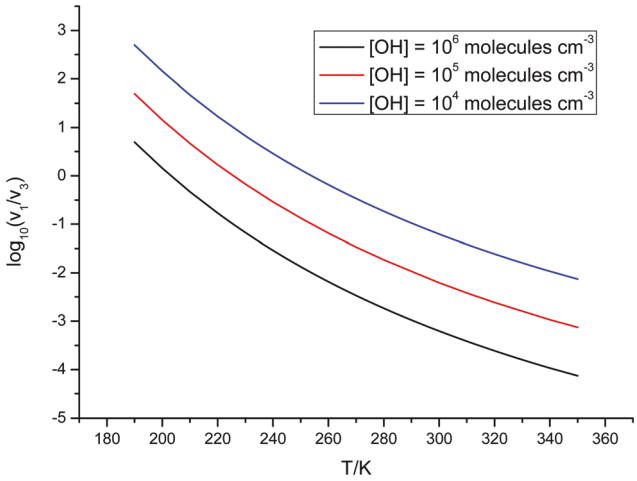

Fig. 4 The rate ratio ν_1/ν_3 for the H_2SO_4 concentration (1×10^8 molecules cm^{-3}) and H_2O concentration (3.8×10^{17} molecules cm^{-3}) at different temperatures and different OH concentrations.

3.4 Atmospheric implications

In gas-phase reactions of the atmosphere, previous investigations have shown that the dominant sink of CH_3CHO is its reaction with OH. Therefore, it is of great importance to discuss the rate ratio between $H_2SO_4\cdots H_2O + CH_3CHO$ and CH_3CHO + OH as shown in eqn (11),

$$\frac{\nu_1}{\nu_3} = \frac{K_{eq2}k_3[H_2SO_4][H_2O][CH_3CHO]}{k_6[OH][CH_3CHO]} = \frac{K_{eq2}k_3[H_2O][H_2SO_4]}{k_6[OH]} \quad (11)$$

where k_6 is the rate constant of the OH + CH_3CHO reaction, which is obtained from the experimental results. The rate ratio ν_1/ν_3 depends on the H_2O, OH, and H_2SO_4 concentrations in the atmosphere, which are provided in Fig. 4. For example, when the concentrations of water[28] at the relative humidity of 50% and OH[66] are 3.8×10^{17} and 1×10^6 molecules cm^{-3}, respectively, and the gas-phase concentration of sulfuric acid exceeds 10^8 molecules cm^{-3}, the $H_2SO_4\cdots H_2O + CH_3CHO$ reaction can compete well with the OH + CH_3CHO reaction. However, the gas-phase concentration of H_2SO_4 in the atmosphere is in the range of 10^4 to 4×10^8 molecules cm^{-3}.[67–69] Consequently, the gas-phase hydrolysis of CH_3CHO catalyzed by H_2SO_4 is negligible in the atmosphere during the day. However, when the OH concentration is decreased to 1×10^4 molecules cm^{-3} during the night,[70] the $H_2SO_4\cdots H_2O + CH_3CHO$ reaction can compete well with the OH + CH_3CHO reaction below 260 K because the rate ratio ν_1/ν_3 is about 0.7 at 260 K as shown in Fig. 4. Thus, the $H_2SO_4\cdots H_2O + CH_3CHO$ reaction can make contribution to the sink of CH_3CHO during the night below 260 K under the conditions of OH (10^4 molecules cm^{-3}), H_2SO_4 (10^8 molecules cm^{-3}), and H_2O (10^8 molecules cm^{-3}).

The calculated results herein also have relevance to secondary organic aerosol formation.[71] The $H_2SO_4\cdots H_2O$ complex has been found in sulfuric acid aerosols.[72,73] Moreover, the experimental results have shown that these aldehyde heterogeneous reactions can be accelerated with an acid catalyst, H_2SO_4, which leads to higher aerosol yields than that in the absence of H_2SO_4 in the seed aerosol.[74] As a result, the $H_2SO_4\cdots H_2O + CH_3CHO$ reaction leads to the formation of the postreactive complex between sulfuric acid and 1,1-ethanediol. This complex has abundant oxygenated functionalization, which can form hydrogen bonds not just with water but other atmospheric molecules. These stable complexes provide excellent nucleation precursor clusters, which finally lead to the formation of secondary organic aerosols.

4. Conclusions

In this article, the hydrolysis of CH_3CHO catalyzed by sulfuric acid was investigated using the CCSD(T)-F12a/VTZ-F12//M06-2X/MG3S theoretical method, the validated MPWB1K functional with the MG3S basis set for direct kinetics calculations, and canonical variational transition state theory with anharmonicity and small-curvature tunneling for rate constants. In theory, we show that the CCSD(T)-F12a theoretical method with the VTZ-F12 basis set is very close to CCSD(T)/CBS in the hydrolysis of CH_3CHO. Moreover, the post-CCSD(T) calculations are not required for the hydrolysis of CH_3CHO. As for the $CH_3CHO + H_2O + H_2SO_4$ reaction, the main entrance channel is the reaction of the $H_2SO_4\cdots H_2O$ complex with CH_3CHO. Additionally, we show that sulfuric acid plays a strong catalytic role in the hydrolysis of CH_3CHO because the energy barrier of the hydrolysis of CH_3CHO is reduced from 37.21 kcal mol^{-1} to −9.79 kcal mol^{-1} relative to the respective separate reactants.

In the gas-phase reactions of the atmosphere, the importance of the $H_2SO_4\cdots H_2O + CH_3CHO$ reaction depends on temperature as well as the concentrations of H_2O, H_2SO_4, and OH. We show that the $H_2SO_4\cdots H_2O + CH_3CHO$ reaction can play an important role as a sink of CH_3CHO below 260 K when the OH concentration is about 10^4 molecules cm^{-3}, which occurs at night, the H_2SO_4 concentration is about 10^8 molecules cm^{-3}, and the H_2O concentration is about 10^{17} molecules cm^{-3}. In addition, the $H_2SO_4\cdots H_2O + CH_3CHO$ reaction may play an important role in the formation of secondary organic aerosols.

The findings of the present work not only show a specific reaction for the reaction mechanism and kinetics, but also show that sulfuric acid can promote the hydrolysis of CH_3CHO. Thus, the present investigation should have wide applications in the hydrolysis of atmospheric molecules such as butanal, hexanal, octanal, and decanal.

Conflicts of interest

The authors declare no competing financial interest.

Acknowledgements

This work was supported in part by the National Natural Science Foundation of China (41775125), by the Science and Technology Foundation of Guizhou Province & Guizhou Minzu University, China ([2015]7211), and by the Science and

Technology Foundation of Guizhou Provincial Department of Education, China ([2015]350). The authors also thank Junwei Lucas Bao from the University of Minnesota for fitting the rate constants and discussing the nonmonotonic character of the rate constant.

References

1 H. B. Singh, L. J. Salas, R. B. Chatfield, E. Czech, A. Fried, J. Walega, M. J. Evans, B. D. Field, D. J. Jacob, D. Blake, B. Heikes, R. Talbot, G. Sachse, J. H. Crawford, M. A. Avery, S. Sandholm and H. Fuelberg, *J. Geophys. Res.: Atmos.*, 2004, **109**, D15S07.
2 D. B. Millet, A. Guenther, D. A. Siegel, N. B. Nelson, H. B. Singh, J. A. de Gouw, C. Warneke, J. Williams, G. Eerdekens, V. Sinha, T. Karl, F. Flocke, E. Apel, D. D. Riemer, P. I. Palmer and M. Barkley, *Atmos. Chem. Phys.*, 2010, **10**, 3405–3425.
3 J. Slemr, W. Junkermann and A. Volz-Thomas, *Atmos. Environ.*, 1996, **30**, 3667–3676.
4 Y.-N. Lee, X. Zhou and K. Hallock, *J. Geophys. Res.: Atmos.*, 1995, **100**, 25933–25944.
5 K. F. Ho, S. S. H. Ho, W. T. Dai, J. J. Cao, R.-J. Huang, L. Tian and W. J. Deng, *Environ. Monit. Assess.*, 2014, **186**, 2835–2849.
6 S. M. Corrêa, E. M. Martins and G. Arbilla, *Atmos. Environ.*, 2003, **37**, 23–29.
7 D. Grosjean, A. H. Miguel and T. M. Tavares, *Atmos. Environ., Part B*, 1990, **24**, 101–106.
8 J. M. Roberts, *Atmos. Environ., Part A*, 1990, **24**, 243–287.
9 J.-F. Müller and G. Brasseur, *J. Geophys. Res.: Atmos.*, 1999, **104**, 1705–1715.
10 R. Atkinson, D. L. Baulch, R. A. Cox, J. N. Crowley, R. F. Hampson, R. G. Hynes, M. E. Jenkin, M. J. Rossi, J. Troe and I. Subcommittee, *Atmos. Chem. Phys.*, 2006, **6**, 3625–4055.
11 D. U. Andrews, B. R. Heazlewood, A. T. Maccarone, T. Conroy, R. J. Payne, M. J. T. Jordan and S. H. Kable, *Science*, 2012, **337**, 1203–1206.
12 J. L. Axson, K. Takahashi, D. O. De Haan and V. Vaida, *Proc. Natl. Acad. Sci. U. S. A.*, 2010, **107**, 6687–6692.
13 B. Long, Z. W. Long, Y. B. Wang, X. F. Tan, Y. H. Han, C. Y. Long, S. J. Qin and W. J. Zhang, *ChemPhysChem*, 2012, **13**, 323–329.
14 M. K. Hazra and A. Sinha, *J. Am. Chem. Soc.*, 2011, **133**, 17444–17453.
15 F.-Y. Liu, X.-F. Tan, Z.-W. Long, B. Long and W.-J. Zhang, *RSC Adv.*, 2015, **5**, 32941–32949.
16 J. Liu, S. Fang, Z. Wang, W. Yi, F. M. Tao and J. Y. Liu, *Environ. Sci. Technol.*, 2015, **49**, 13112–13120.
17 M. K. Louie, J. S. Francisco, M. Verdicchio, S. J. Klippenstein and A. Sinha, *J. Phys. Chem. A*, 2015, **119**, 4347–4357.
18 H. A. Rypkema, A. Sinha and J. S. Francisco, *J. Phys. Chem. A*, 2015, **119**, 4581–4588.
19 B. Long, X.-F. Tan, C.-R. Chang, W.-X. Zhao, Z.-W. Long, D.-S. Ren and W.-J. Zhang, *J. Phys. Chem. A*, 2013, **117**, 5106–5116.
20 M. K. Hazra, J. S. Francisco and A. Sinha, *J. Phys. Chem. A*, 2014, **118**, 4095–4105.
21 M. K. Hazra, J. S. Francisco and A. Sinha, *J. Phys. Chem. A*, 2013, **117**, 11704–11710.
22 M. Torrent-Sucarrat, J. S. Francisco and J. M. Anglada, *J. Am. Chem. Soc.*, 2012, **134**, 20632–20644.
23 B. Long, X.-F. Tan, Y.-B. Wang, J. Li, D.-S. Ren and W.-J. Zhang, *ChemistrySelect*, 2016, **1**, 1421–1430.
24 M. Kumar, A. Sinha and J. S. Francisco, *Acc. Chem. Res.*, 2016, **49**, 877–883.
25 B. Long, C.-R. Chang, Z.-W. Long, Y.-B. Wang, X.-F. Tan and W.-J. Zhang, *Chem. Phys. Lett.*, 2013, **581**, 26–29.
26 W. Xu, M. Gomez-Hernandez, S. Guo, J. Secrest, W. Marrero-Ortiz, A. L. Zhang and R. Zhang, *J. Am. Chem. Soc.*, 2014, **136**, 15477–15480.
27 Z. Li, A. N. Schwier, N. Sareen and V. F. McNeill, *Atmos. Chem. Phys.*, 2011, **11**, 11617–11629.
28 B. Long, J. L. Bao and D. G. Truhlar, *J. Am. Chem. Soc.*, 2016, **138**, 14409–14422.
29 B. Chan and L. Radom, *J. Chem. Theory Comput.*, 2015, **11**, 2109–2119.
30 T. B. Adler, G. Knizia and H.-J. Werner, *J. Chem. Phys.*, 2007, **127**, 221106.
31 G. Knizia, T. B. Adler and H.-J. Werner, *J. Chem. Phys.*, 2009, **130**, 054104.
32 K. A. Peterson, T. B. Adler and H.-J. Werner, *J. Chem. Phys.*, 2008, **128**, 084102.
33 K. E. Yousaf and K. A. Peterson, *J. Chem. Phys.*, 2008, **129**, 184108.
34 G. D. Purvis and R. J. Bartlett, *J. Chem. Phys.*, 1982, **76**, 1910–1918.
35 T. H. Dunning, *J. Chem. Phys.*, 1989, **90**, 1007–1023.
36 E. A. Salter, G. W. Trucks and R. J. Bartlett, *J. Chem. Phys.*, 1989, **90**, 1752–1766.
37 Y. Zhao and D. G. Truhlar, *Theor. Chem. Acc.*, 2008, **120**, 215–241.
38 B. J. Lynch, Y. Zhao and D. G. Truhlar, *J. Phys. Chem. A*, 2003, **107**, 1384–1388.
39 J. Elm, M. Bilde and K. V. Mikkelsen, *J. Chem. Theory Comput.*, 2012, **8**, 2071–2077.
40 H. P. Hratchian and H. B. Schlegel, *J. Chem. Theory Comput.*, 2005, **1**, 61–69.
41 H. P. Hratchian and H. B. Schlegel, *J. Chem. Phys.*, 2004, **120**, 9918–9924.
42 Y. Zhao and D. G. Truhlar, *J. Phys. Chem. A*, 2004, **108**, 6908–6918.
43 J. L. Bao, P. Sripa and D. G. Truhlar, *Phys. Chem. Chem. Phys.*, 2016, **18**, 1032–1041.
44 Y. P. Liu, G. C. Lynch, T. N. Truong, D. H. Lu, D. G. Truhlar and B. C. Garrett, *J. Am. Chem. Soc.*, 1993, **115**, 2408–2415.
45 D. G. Truhlar and B. C. Garrett, *Annu. Rev. Phys. Chem.*, 1984, **35**, 159–189.
46 A. Fernández-Ramos, J. A. Miller, S. J. Klippenstein and D. G. Truhlar, *Chem. Rev.*, 2006, **106**, 4518–4584.
47 T. Yu, J. Zheng and D. G. Truhlar, *J. Phys. Chem. A*, 2012, **116**, 297–308.

48 J. Zheng and D. G. Truhlar, *Faraday Discuss.*, 2012, **157**, 59–88.
49 J. L. Bao, P. Sripa and D. G. Truhlar, *Phys. Chem. Chem. Phys.*, 2016, **18**, 1032–1041.
50 J. L. Bao, R. Meana-Paneda and D. G. Truhlar, *Chem. Sci.*, 2015, **6**, 5866–5881.
51 J. L. Bao and D. G. Truhlar, *Chem. Soc. Rev.*, 2017, **46**, 7548–7596.
52 B. Long, X.-F. Tan, J. L. Bao, D.-M. Wang and Z.-W. Long, *Int. J. Chem. Kinet.*, 2016, **49**, 130–139.
53 I. M. Alecu, J. Zheng, Y. Zhao and D. G. Truhlar, *J. Chem. Theory Comput.*, 2010, **6**, 2872–2887.
54 J. Zheng, T. Yu, E. Papajak, I. M. Alecu, S. L. Mielke and D. G. Truhlar, *Phys. Chem. Chem. Phys.*, 2011, **13**, 10885–10907.
55 J. Zheng and D. G. Truhlar, *J. Chem. Theory Comput.*, 2013, **9**, 1356–1367.
56 J. Zheng, R. Meana-Pañeda and D. G. Truhlar, *Comput. Phys. Commun.*, 2013, **184**, 2032–2033.
57 M. J. Frisch, G. W. Trucks, H. B. Schlegel, G. E. Scuseria, M. A. Robb, J. R. Cheeseman, G. Scalmani, V. Barone, B. Mennucci, G. A. Petersson, H. Nakatsuji, M. Caricato, X. Li, H. P. Hratchian, A. F. Izmaylov, J. Bloino, G. Zheng, J. L. Sonnenberg, M. Hada, M. Ehara, K. Toyota, R. Fukuda,J. Hasegawa, M. Ishida, T. Nakajima, Y. Honda, O. Kitao, H. Nakai, T. Vreven, J. A. Montgomery Jr, J. E. Peralta, F. Ogliaro, M. Bearpark, J. J. Heyd, E. Brothers, K. N. Kudin, V. N. Staroverov, R. Kobayashi, J. Normand, K. Raghavachari, A. Rendell, J. C. Burant, S. S. Iyengar, J. Tomasi, M. Cossi, N. Rega, J. M. Millam, M. Klene, J. E. Knox, J. B. Cross, V. Bakken, C. Adamo, J. Jaramillo, R. Gomperts, R. E. Stratmann, O. Yazyev, A. J. Austin, R. Cammi, C. Pomelli, J. W. Ochterski, R. L. Martin, K. Morokuma, V. G. Zakrzewski, G. A. Voth, P. Salvador, J. J. Dannenberg, S. Dapprich, A. D. Daniels, Ö. Farkas, J. B. Foresman, J. V. Ortiz, J. Cioslowski and D. J. Fox, *Gaussian 09, revision C.01*, Gaussian, Inc., Wallingford, CT, 2010, http://www.gaussian.com/g_prod/g09.html.
58 H.-J. Werner, P. J. Knowles, G. Knizia, F. R. Manby, M. Schütz, P. Celani, W. Györffy, D. Kats, T. Korona, R. Lindh, A. Mitrushenkov, G. Rauhut, K. R. Shamasundar, T. B. Adler, R. D. Amos, A. Bernhardsson, A. Berning, D. L. Cooper, M. J. O. Deegan, A. J. Dobbyn, F. Eckert, E. Goll, C. Hampel, A. Hesselmann, G. Hetzer, T. Hrenar, G. Jansen, C. Köppl, Y. Liu, A. W. Lloyd, R. A. Mata, A. J. May, S. J. McNicholas, W. Meyer, M. E. Mura, A. Nicklaß, D. P. O'Neill, P. Palmieri, D. Peng, K. Pflüger, R. Pitzer, M. Reiher, T. Shiozaki, H. Stoll, A. J. Stone, R. Tarroni, T. Thorsteinsson and M. Wang, *MOLPRO, version 2012.1*, a package of ab initio programs, 2012, http://www.molpro.net.
59 Z. Rolik, L. Szegedy, I. Ladjánszki, B. Ladóczki and M. Kállay, *J. Chem. Phys.*, 2013, **139**, 094105.
60 M. Kállay, Z. Rolik, I. Ladjánszki, L. Szegedy, B. Ladóczki, J. Csontos and B. Kornis, *MRCC, A Quantum Chemical Program Suite*, 2015, http://www.mrcc.hu/.
61 J. Zheng, J. L. Bao, R. Meana-Pañeda,S. Zhang, B. J. Lynch, J. C. Corchado, Y.-Y. Chuang, P. L. Fast, W.-P. Hu, Y.-P. Liu, G. C. Lynch, K. A. Nguyen, C. F. Jackels, A. F. Ramos, B. A. Ellingson, V. S. Melissas, J. Vill_a, I. Rossi, E. L. Coitino, J. Pu, T. V. Albu, R. Steckler, B. C. Garrett, A. D. Isaacson and D. G. Truhlar, *Polyrate2016-2A*, University of Minnesota, Minneapolis, 2016, https://comp.chem.umn.edu/polyrate/.
62 J. Zheng, S. Zhang, J. C. Corchado,R. Meana-Pañeda, Y.-Y. Chuang, E. L. Coitiño, B. A. Ellingson and D. G. Truhlar, *Gaussrate 2016*, University of Minnesota, Minneapolis, 2016, https://comp.chem.umn.edu/gaussrate/.
63 M.-L. Wei, X.-F. Tan, Z.-W. Long and B. Long, *RSC Adv.*, 2017, **7**, 56211–56219.
64 J. Demaison, M. Herman, J. Liévin and H. D. Rudolph, *J. Phys. Chem. A*, 2007, **111**, 2602–2609.
65 D. G. Truhlar, *J. Chem. Educ.*, 1978, **55**, 309–311.
66 B. Long, J. L. Bao and D. G. Truhlar, *Phys. Chem. Chem. Phys.*, 2017, **19**, 8091–8100.
67 F. L. Eisele and D. J. Tanner, *J. Geophys. Res.: Atmos.*, 1993, **98**, 9001–9010.
68 S. Mikkonen, S. Romakkaniemi, J. N. Smith, H. Korhonen, T. Petäjä, C. Plass-Duelmer, M. Boy, P. H. McMurry, K. E. J. Lehtinen, J. Joutsensaari, A. Hamed, R. L. Mauldin Iii, W. Birmili, G. Spindler, F. Arnold, M. Kulmala and A. Laaksonen, *Atmos. Chem. Phys.*, 2011, **11**, 11319–11334.
69 T. Petäjä, I. R. L. Mauldin, E. Kosciuch, J. McGrath, T. Nieminen, P. Paasonen, M. Boy, A. Adamov, T. Kotiaho and M. Kulmala, *Atmos. Chem. Phys.*, 2009, **9**, 7435–7448.
70 M. A. H. Khan, M. J. Ashfold, G. Nickless, D. Martin, L. A. Watson, P. D. Hamer, R. P. Wayne, C. E. Canosa-Mas and D. E. Shallcross, *Atmos. Sci. Lett.*, 2008, **9**, 140–146.
71 C. Tong, M. Blanco, W. A. Goddard and J. H. Seinfeld, *Environ. Sci. Technol.*, 2006, **40**, 2333–2338.
72 S. B. Couling, K. J. Sully and A. B. Horn, *J. Am. Chem. Soc.*, 2003, **125**, 1994–2003.
73 S. B. Couling, J. Fletcher, A. B. Horn, D. A. Newnham, R. A. McPheat and R. Gary Williams, *Phys. Chem. Chem. Phys.*, 2003, **5**, 4108–4113.
74 M. Jang and R. M. Kamens, *Environ. Sci. Technol.*, 2001, **35**, 4758–4766.